One-step deposition of nano-to-micron-scalable, high-quality digital image correlation patterns for high-strain in-situ multi-microscopy testing

Received: 26 April 2019 | Revised: 23 July 2019 | Accepted: 3 August 2019

DOI: 10.1111/str.12330

FULL PAPER

WILEY strain

One-step deposition of nano-to-micron-scalable, high-quality digital image correlation patterns for high-strain *in-situ* multi-microscopy testing

J.P.M. Hoefnagels | **M.P.F.H.L. van Maris** | **T. Vermeij**

Department of Mechanical Engineering, Eindhoven University of Technology, Eindhoven, The Netherlands

Correspondence
J. P. M. Hoefnagels, Department of Mechanical Engineering, Eindhoven University of Technology, Eindhoven, The Netherlands.
Email: j.p.m.hoefnagels@tue.nl

Funding information
Partnership Program of the Materials innovation institute (M2i), Grant/Award Number: S17012b; Netherlands Organization for Scientific Research

Abstract

Digital image correlation (DIC) is of vital importance in the field of experimental mechanics, yet producing suitable DIC patterns for demanding *in-situ* (micro) mechanical tests remains challenging, especially for ultrafine patterns, despite the large number of patterning techniques reported in the literature. Therefore, we propose a simple, flexible, one-step technique (only requiring a conventional physical vapour deposition machine) to obtain scalable, high-quality, robust DIC patterns, suitable for a range of microscopic techniques, by deposition of a low-melting temperature solder alloy in the so-called island growth mode, without elevating the substrate temperature. Proof of principle is shown by (near-)room temperature deposition of InSn patterns, yielding highly dense, homogeneous DIC patterns over large areas with a feature size that can be tuned from as small as ~10 nm to ~2 μm and with control over the feature shape and density by changing the deposition parameters. Pattern optimisation, in terms of feature size, density, and contrast, is demonstrated for imaging with atomic force microscopy, scanning electron microscopy, optical profilometry, and optical microscopy. Moreover, the performance of the InSn DIC patterns and their robustness to large deformations is validated in two challenging case studies of *in-situ* micromechanical testing: (a) self-adaptive isogeometric digital height correlation of optical surface height profiles of a coarse, bimodal InSn pattern providing microscopic 3D deformation fields (illustrated for delamination of Al stretchable interconnects on a PI substrate) and (b) DIC on scanning electron microscopy images of a much finer InSn pattern allowing quantification of high strains near fracture locations (illustrated for rupture of a polycrystalline Fe foil). As such, the high controllability, performance, and scalability of the DIC patterns, created by island growth of a solder alloy, offer a promising step towards more routine DIC-based *in-situ* micromechanical testing.

KEYWORDS

DIC pattern, digital image correlation, experimental mechanics, *in-situ* micromechanical testing, optical profilometry, scanning electron microscopy

1 | INTRODUCTION

Digital image correlation (DIC) is an essential technique in today's field of experimental mechanics. It allows full-field measurement of displacements, from which, for example, strains can be derived, with high (subpixel) accuracy, and can be applied on a wide range of tests without requiring direct (mechanical) contact, while being highly robust to noise.[1–3] DIC has proven to be a broad multipurpose method, being employed in a wide range of applications and investigations, ranging from analysis of objects as large as airplanes and bridges[4,5] to detailed identification of crystal plasticity and damage mechanisms on the microscale or even nanoscale.[6,7] Moreover, DIC is extremely versatile, as it can be performed on various types of images, acquired with regular camera, optical microscope (e.g., Carroll et al.,[8] and Ruybalid et al.,[9]), scanning electron microscope (SEM; e.g., Kammers & Daly[10]), or transmission electron microscopy.[11] Yet DIC is not limited to (2D) in-plane displacement measurements but can readily be extended to measure the 3D displacement field of a surface, with (multicamera) stereo-DIC (e.g., Wang et al.,[12]) or digital height correlation (DHC), where the surface height profiles can be acquired with an optical profilometre (e.g., Bertin et al.,[6] and Bergers et al.,[13]) or an atomic force microscope (AFM; e.g., Li et al.,[14] and Xu et al.,[15]). DIC can even be applied to measure the 3D displacement field of a volume, for example, by correlating X-ray computed tomography images (e.g., Bay et al.,[16]). The correlation on the acquired images or height data is traditionally performed through the correlation of local regions (subsets or windows), sometimes called "local DIC." In contrast, in "global DIC," the correlation is performed over the complete field of view (FOV), whereas typical material continuity is assumed over the complete FOV.[17] Finally, these full-field measurements can directly be coupled in various ways to numerical simulations or theoretical models for the identification of (material) parameters (See e.g. Refs.[18–21]).

A crucial requisite for proper DIC analysis is a high-quality pattern that provides enough contrast at the scale of interest (locally and/or globally) for the DIC algorithm to be able to track. Although the natural features of the sample are satisfactory in some cases, for example, for multiphase materials,[22–24] their change during the experiment is often detrimental to the quality of the correlation.[25] Therefore, in most cases, high-quality DIC analysis requires application of a pattern on the sample surface. For optimal correlation accuracy, the pattern should consist of a homogeneous, high-density distribution of features (speckles) with the size of a few pixels in order to achieve a small pattern correlation length and high mean intensity gradient.[26,27] Therefore, the patterns must be tailored to the specific requirements of the experiment, such as the type of microscopy (or imaging) technique, the length scale of observation (both the smallest scale and the total FOV) at which the correlation should be performed, and the ability to sustain high (localised) strains without showing pattern degradation or changes. Application of such a high-quality pattern is typically far from trivial, often limiting the spatial resolution and accuracy of the displacement and strain field, especially for the nanoscale patterns needed for high-magnification experiments. Moreover, the pattern must be applied without altering (the microstructure and deformation of) the underlying specimen in any way or form. For example, a heat treatment can easily cause undetected rearrangement of dislocations in a (poly-)crystal thereby affecting the micromechanical behaviour, which obviously should be avoided.

For DIC of images obtained with a regular camera (or low-magnification optical microscope), simple techniques such as spray painting or using an airbrush typically provide a good pattern,[28] yet correlations at higher magnification (high-magnification optical microscopy, optical profilometry, SEM, or AFM) place more stringent requirements on the DIC pattern. In the literature, a large number of techniques exist to apply microscale or nanoscale DIC patterns.[29–40] Two types of nanoscale patterning techniques stand out. First, nanoparticles (of different materials and sizes) can be dispersed over the sample surface. This can be achieved, for example, by the so-called drop casting or mistification of droplets of nanoparticles in a solvent; however, a homogeneous particle density without clusters is notoriously difficult to achieve due to Marangoni flow in the droplets while the solvent evaporates at the surface.[32] Therefore, alternative particle dispersion techniques have been proposed, for example, (wet) self-assembly of gold particles[33,34] or pressing of colloidal silica particles into the surface during chemically assisted polishing.[35] Although these alternative particle dispersion techniques have clearly proven their merits, they are still sensitive to clustering of the particles, which can only be completely avoided at the expense of a lower feature density. Moreover, they rely on (lengthy or cumbersome) processing steps that are sensitive to operator input; therefore, good reproducibility is not readily achieved. Second, nanoscale pattern application by deposition of a metal (e.g., gold or silver) has been proposed, where first one or more layers of homogeneous thickness are deposited followed by a heat treatment (at high temperature and/or assisted by a chemical reaction) to instigate remodelling of the layer into separate islands.[29,36,37,40] The importance of all of these patterning techniques to the community is undisputed, as can be clearly seen from the high number of citations to most of the above-mentioned references. Yet truly ultrafine patterns (with a feature size

around 10 nm) are not readily achieved. Moreover, even the best patterns typically still contain significant pattern-free area between the particles and islands, often resulting in nearly black and white images with few intermediate grey values. Moreover, most of these techniques have been optimised for one specific microscopy technique, length scale, or sample geometry, without demonstrated flexibility for subtle modifications in size, size range, density, etc. Finally, as explained above, heat treatments, pressure, or chemical reactions are best avoided. Considering these concerns, there is still a clear interest for an easy-to-implement, (near-)room temperature, one-step patterning method that can produce high-quality microscale to nanoscale DIC patterns with high reproducibility. It is important that the processing method provides sufficient freedom to allow uncomplicated tuning of the shape and size of the pattern features, in order to adhere to a wide range of DIC environments and microscopic techniques, without being constrained to low strains.

In this work, we explore the suitability of one-step deposition of metal islands (using physical vapour deposition [PVD]) in the so-called island growth (Volmer–Weber) deposition mode, as opposed to first depositing a homogeneous layer that subsequently requires thermal/chemical processing. Island growth requires a large surface diffusion length of the metal adatoms that typically only occurs at a very high substrate temperature.[41–43] Here, however, we set the requirement that the pattern must be applied through a single short-duration deposition step without requiring substrate temperature elevation (also because most commercial deposition systems come without substrate temperature control). Without specimen heating, direct island growth may still be achieved by selecting (a) metal adatoms with a high surface mobility (e.g., [eutectic] low-melting temperature [solder] alloys) in combination with (b) a plasma that boosts the adatom surface diffusion length as each adatoms receives the kinetic energy from multiple ions. By sufficiently increasing adatom surface diffusion length, the growth of islands is activated from the start of the deposition. An added advantage of island growth would be that, for very short deposition times, the islands should be very small and nearly touching each other, whereas by increasing the deposition time, the size of the islands can be tuned to the DIC application at hand. In this work, a simple DC magnetron sputter deposition machine is employed to demonstrate that high-quality patterns are easily accessible in a reproducible manner, whereas it is shown that good patterns can be achieved for a wide range of deposition/plasma settings. This makes the exact specifications of the deposition machine unimportant.

2 | PATTERNING METHOD AND RESULTS

A Torr CRC-600 system without substrate temperature control is used to perform planar direct current magnetron sputter deposition. This is a PVD method in which, under vacuum, (clusters of) atoms are ejected from a target, by positively charged Ar ions, and accelerated towards the sample surface, where they collect to ultimately form a layer, see Figure 1. We believe, however, that any sputter deposition machine could have been used. As explained in Section 1, the feature (island) size is largely governed by the mobility of the metal adatoms on the surface, that is, the adatom surface diffusion length, to form large islands. According to Jung et al.,[43] the adatom mobility is increased when a low pressure is administered, because the target atoms retain more kinetic energy during the transport from target to substrate due to fewer collisions with the background gas. Also, high temperatures of the adatoms with respect to the melting temperature of the target material are reported to increase the adatom mobility and therefore to provoke island growth.[43]

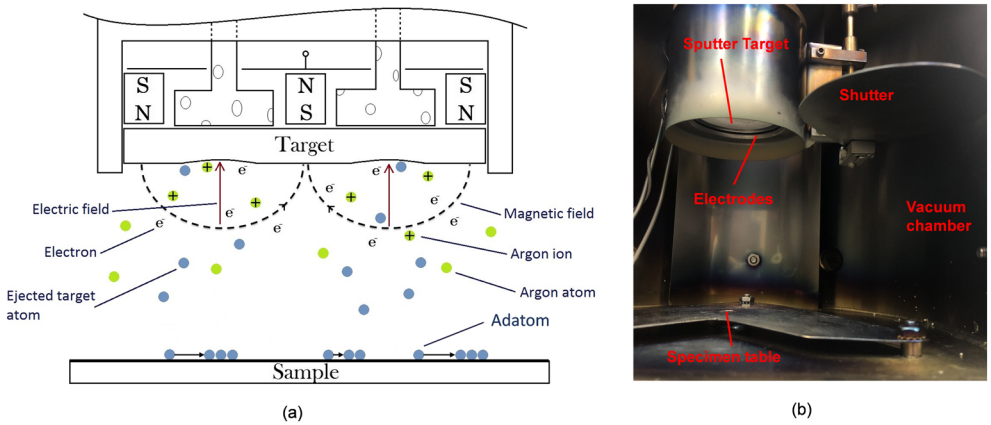

FIGURE 1 (a) Schematic illustration of the direct current magnetron sputter deposition process and (b) image from inside the deposition chamber with specifications of relevant components

Here, however, the aim is to avoid substrate temperature elevation; therefore, instead, a solder alloy with (very) low-melting temperature is selected. Accordingly, two deposition materials are explored in this study: (a) a simple solder alloy (SAC305, Sn96.5Ag3Cu0.5, melting temperature 217°C) and (b) an InSn alloy (In52Sn48, melting temperature 118°C), which are both melted in a crucible for insertion as a target in the deposition system. The morphology of the DIC pattern features can be manipulated by varying several processing parameters of the deposition process: the chamber pressure, the plasma current, and the sputter time. Finally, although the used deposition system comes without a substrate heater, the effect of a mild substrate temperature elevation on the island morphology is still explored, for some of the patterns, by inserting a heated block as substrate holder.

First, we try to achieve a DIC pattern using the SAC alloy on a Si wafer, by performing a deposition at a chamber pressure of 100 mTorr and a sputter current of 20 mA for 3 min, with the substrate at room temperature. For this first deposition try, no surface features could be observed in the SEM. Therefore, the sample was shortly heated to 300°C, with the final result shown in Figure 2. A pattern with ultrafine nanoscale features is observed with a density and contrast that appears to be challenging those reported in the literature, thereby making this pattern certainly suitable for *in-situ* SEM testing at high magnification for submicron DIC resolution. However, the clusters, which probably have been extracted directly from the target, and the dark residue spots, which likely were induced by oxidation during the heat treatment, show that the pattern is not perfect. Most importantly, the postdeposition heat treatment, which is required to remodel the homogeneous SAC alloy layer into islands, should be avoided as explained in Section 1. Therefore, further attempts with the SAC alloy were abandoned.

Next, the InSn alloy was tested, as it has an even lower melting temperature of only 118°C and is, therefore, expected to provide a much larger adatom surface diffusion length. For each of the wide range of deposition settings that were initially explored with the substrate at room temperature, a fine scale pattern of islands was deposited. This shows that the concept of direct island growth of a low-melting temperature metal is indeed feasible and that this concept is not limited to a narrow range of deposition parameters. Subsequently, a representative range of InSn DIC patterns has been deposited using the six different sets of deposition parameters that are provided in Table 1. Each resulting pattern is imaged in a SEM at high resolution, as shown in Figure 3. As can be seen, all deposition settings, that is, the substrate material (Si wafer and polyimide [PI]; and Fe in the second test case below), sputter current, chamber pressure, sputter time, and substrate temperature, were varied, confirming that high-quality patterns can be achieved for a wide range of deposition/plasma settings (and most probably different types of deposition machines). From these SEM images, the feature size range is qualitatively estimated and included in Table 1. The table also shows the correlation length, which is calculated as the standard deviation of the Gaussian function fitted to the peak in the autocorrelation function of the pattern. Each pattern is homogeneous over a very large area. Moreover, each pattern has a distinct length scale, as seen from both the feature size range and correlation length. The feature sizes range between ~10 nm and ~2 μm, whereas the correlation length varies between 6 and 159 nm. The difference between feature size and correlation length can be

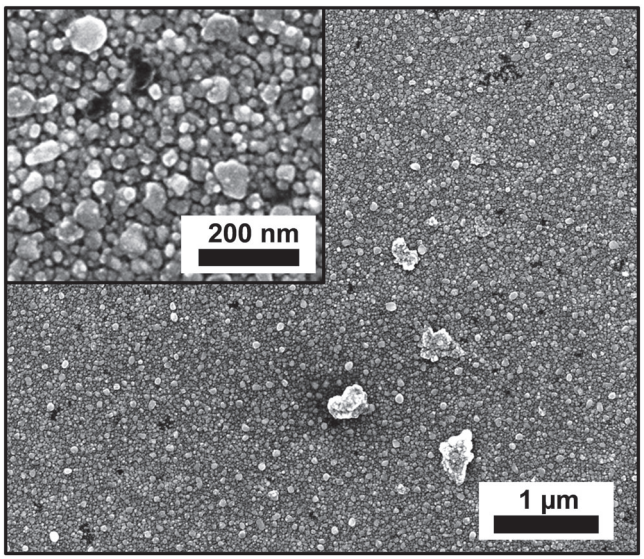

FIGURE 2 SAC pattern, with postdeposition heat treatment to 300°C, imaged in secondary electron mode in a FEI Quanta 600 SEM, showing a highly dense nanoscale pattern but with a significant amount of large clusters and dark residue spots

TABLE 1 Deposition parameters and pattern properties for the range of six InSn digital image correlation patterns

Sample	Substrate material	Current (mA)	Pressure (mTorr)	Time (min)	T (°C)	Feature size range (nm)[a]	Correlation length (nm)[b]
a	Si	10	8	5	20	~10 to ~30	6
b	Si	40	100	15	20	~15 to ~60	8
c	Si	15	8	3	20	~20 to ~100	24
d	Si	15	8	5	20	~30 to ~200	33
e	PI	20 and 60	8	2 and 7	80	~100 to ~1,000	62
f	PI	50	8	15	20	~100 to ~2,000	159

Note. For the wide range of deposition settings that were probed, including the six settings in this table, a homogeneous nano-sized pattern is consistently achieved.

[a]Qualitative estimation from scanning electron microscope images in Figure 3. [b]Standard deviation of the Gaussian function fitted to the peak of the autocorrelation function of the patterns from Figure 3.

explained by the fact that the correlation length is sensitive to the sharpness of the edges of the features, which are predominantly smaller than the feature size. The usefulness of these patterns for performing high-quality DIC will be shown below by testing Patterns **c** and **e** in *in-situ* DIC tests using, respectively, SEM and optical profilometry.

Generally, the following effects of the deposition parameters were observed: higher sputter currents and deposition times yield larger features, whereas a higher chamber pressure results in smaller features. Note that, comparing Pattern **a** to Pattern **b**, the sputter current and chamber pressure are both significantly increased, and the size of the features are similar, whereas one can clearly distinguish a difference in morphology between them, with, for example, sharper edges in Pattern **b** than in Pattern **a**. This shows that two deposition parameters can be simultaneously varied to control a single property of the DIC pattern. It also indicates that the patterning method can indeed be well tuned to a demanding imaging technique that might require a specific type of feature size, shape, or contrast. Additionally, when the features become larger, there seems to be a natural development towards a bimodal distribution of island sizes, which can be observed in Patterns **c** and **d** but is especially clear in Patterns **e** and **f**, with ratios between feature sizes of up to 20. Such a bimodal DIC pattern can have large benefits when deformation fields need to be measured at multiple scales, by applying DIC on images using the same pattern but captured at multiple magnifications.[44] Note that these bimodal patterns appear as highly dense, homogeneous patterns when imaged at the lower magnification, as shown in the examples of Figures 4 and 6 below. Therefore, the bimodal character is not detrimental to the pattern quality when imaged at a single magnification that is appropriately selected.

The small features in Pattern **a** suggest that this pattern could also be well suited for DIC on AFM height profiles, in order to conduct DIC with higher spatial resolution than feasible with SEM images, but this would require the pattern to have a sufficient and clear height contrast. To this end, Figure 5 shows an AFM scan (captured with a Digital Instruments DI 3100) of Pattern **a**, clearly confirming the high, homogeneous feature density of this pattern. The features have round shapes, as expected for an "island growth" deposition pattern, with height variations in the range of a few nanometres. Moreover, the side slopes of the features are not too steep, thereby enabling accurate AFM imaging. The height contrast that is observed indeed suggests that Pattern **a** is not only suited for *in-situ* SEM testing but also provides good height contrast for nanoscale DIC using an AFM. This allows, for example, the combined imaging with AFM and SEM during an *in-situ* mechanical test, which has not yet been demonstrated in the literature.

With the increase in feature size from Patterns **a** to **f**, the slope of the side edges of the larger islands inevitably also becomes steeper, which could become a problem for optical profilometry as it needs a courser pattern than AFM. Therefore, with Pattern **e**, an example is shown of a deposition performed at an elevated substrate temperature of 80°C. As expected, the pattern size remains (visibly) unchanged as a result of this relatively small temperature increase, as this is insufficient to significantly increase the adatom surface diffusion length. However, it was found that this mild substrate temperature increase is sufficient to slightly round off the edges of the islands and thus to decrease the side slope angle. This circumvents the need to eliminate incorrect measurements points (NaN's) from the optical surface height profiles, as will be shown in Figure 6 below.

Alternatively, the patterns should also be applicable for DIC in combination with a less complex imaging technique, such as optical microscopy. Hence, we briefly investigated how well, for example, Pattern **e** is suitable for this purpose. To this end, Figure 4 shows Nomarski interference contrast mode images of Pattern **e** at two magnifications (captured with a Zeiss Axioplan 2). Using a 20× objective in Figure 4a, Pattern **e** shows a highly dense and homogeneous pattern

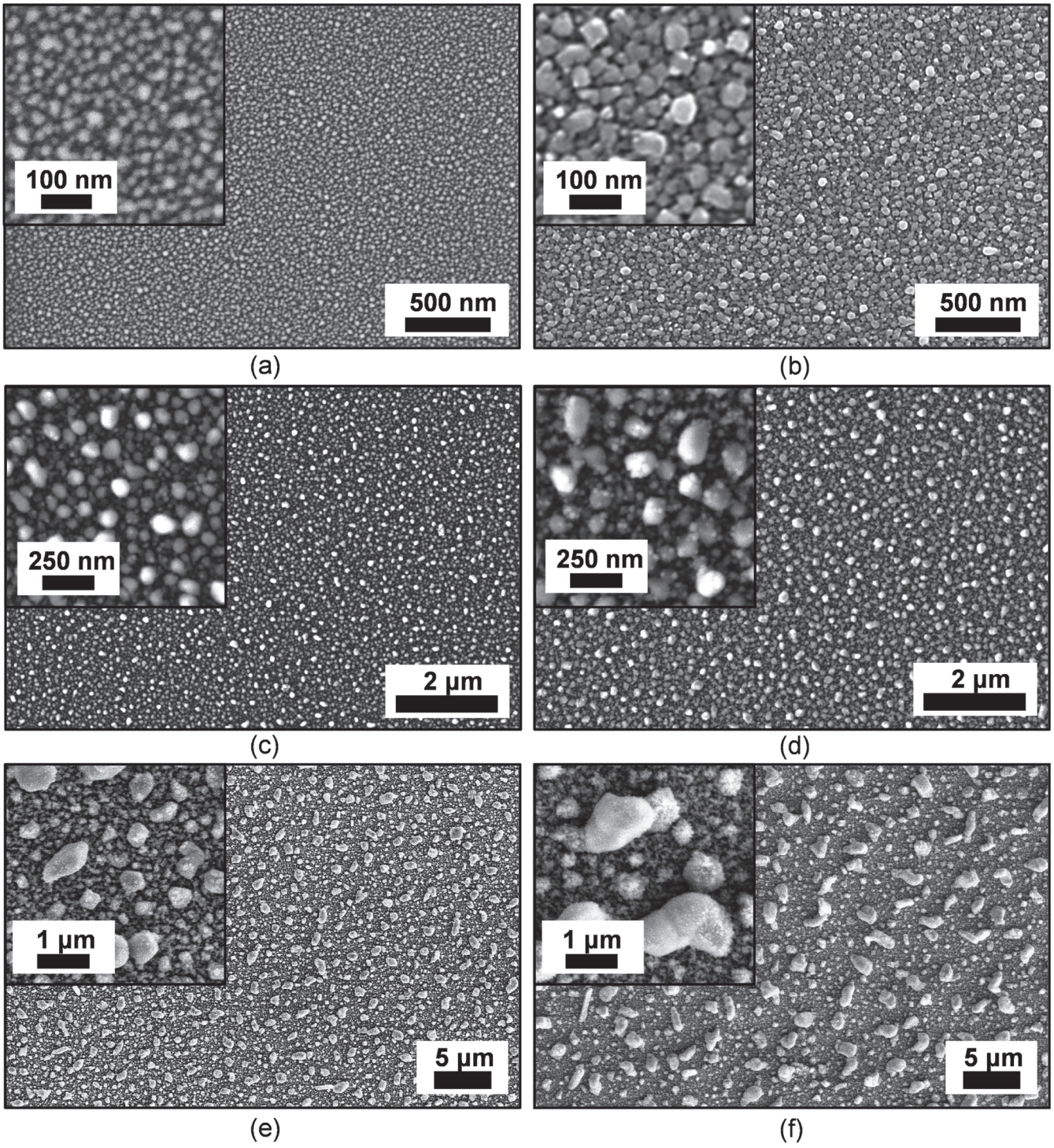

FIGURE 3 Secondary electron scanning electron microscope scans of six different InSn DIC patterns with increasing feature size, produced with the deposition parameters listed in Table 1. Images a, c, and d are captured with a Tescan Mira 3; images b, e, and f are captured using a FEI Quanta 600

over a large area. Moreover, the inset shows that sufficient contrast is retained for DIC on this scale. Additionally, using five times higher magnification in Figure 4b on the same location, smaller details can still be observed with similar quality to the SEM image in Figure 3e, owing to the high sensitivity of Nomarski interference contrast to surface roughness. This example shows that, with a rather simple optical microscope, a single pattern contains sufficient details from submicrometre to millimetre range, confirming the powerful ability of this patterning technique for *in-situ* multiscale DIC experiments. Similarly, Pattern **f** could be used for two-scale imaging with two regular optical cameras.

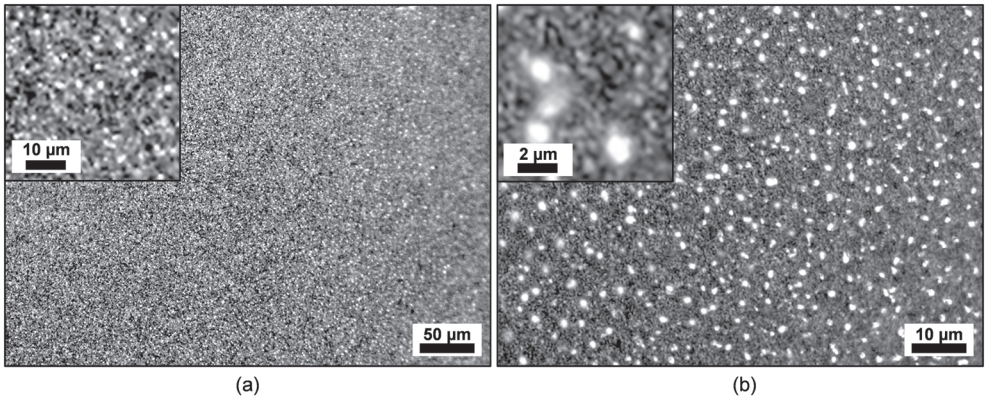

FIGURE 4 Optical microscopy images of InSn digital image correlation Pattern **e**. High contrast on multiple scales is shown with (a) a 20× objective Nomarski Interference Contrast (NIC) image, showing a homogeneous pattern over a large area, and (b) a 100× objective NIC image in the same location, in which submicron-sized features can be distinguished. Note that the blurring on the right side of the images is caused by the out-of-plane curvature of PI foil, which is the substrate of this pattern

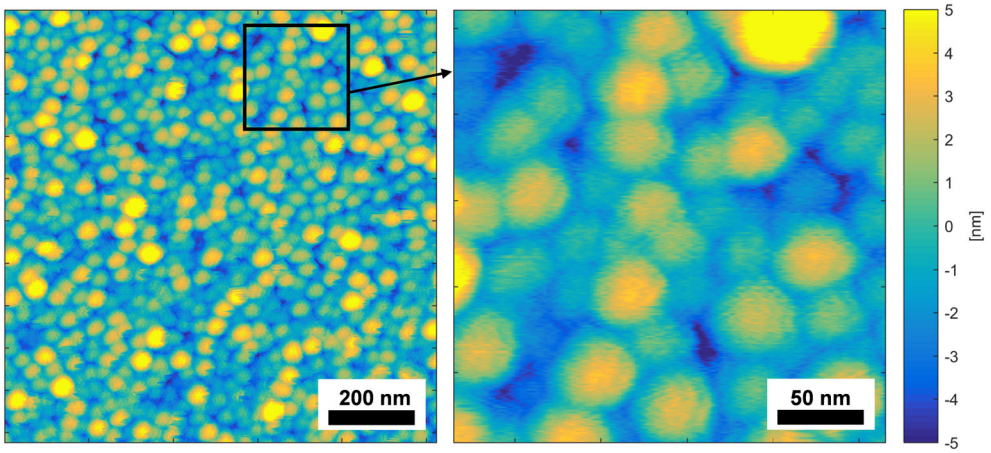

FIGURE 5 Nanoscale atomic force microscope scan of InSn DIC Pattern **a**, from Figure 3a and Table 1

3 | PROOF OF PRINCIPLE: *IN-SITU* OPTICAL PROFILOMETRY AND SEM TESTING

Although all the patterns are expected to perform well during DIC experiments, we demonstrate this with two challenging *in-situ* micromechanical tests analysed with appropriately chosen DIC methods: (I) quantification of the 3D surface displacement field during delamination of a thin Al interconnect adhered to a PI substrate and (II) analysis of micron-scale plasticity, damage localisation, and fracture mechanisms in a polycrystalline Fe foil.

For Case Study I, we are interested in the failure limits of stretchable electronics and, specifically, how the delamination between Al and PI occurs during, for example, a global tensile test. As delamination in this test predominantly yields out-of-plane displacements, stereo-DIC could be applied, to measure the 3D surface displacement field (i.e., the combined in-plane and out-of-plane displacement fields) on the specimen.[45,46] However, for stereo-DIC applied to images captured with an optical stereo microscope, the out-of-plane displacement resolution is limited due to the small viewing angle between the two cameras. Here, however, DHC is applied to surface height profiles measured with an optical profilometre.[6,13,47–49] With this technique, 3D surface displacement fields can be measured with very high out-of-plane displacement resolution (down to a few nanometre[13]), as it uses high-resolution quantitative height data instead of qualitative grey-scale values in the correlation algorithm. The height profile of an as-received sample is shown in Figure 6a, which clearly shows insufficient local contrast for a proper DHC correlation (which is confirmed by preliminary tests, not shown here), whereas the steep edges also show erroneous height measurements, which would be problematic for DHC. Applying InSn Pattern **e** results in the topography in Figure 6b, where it is seen that the side

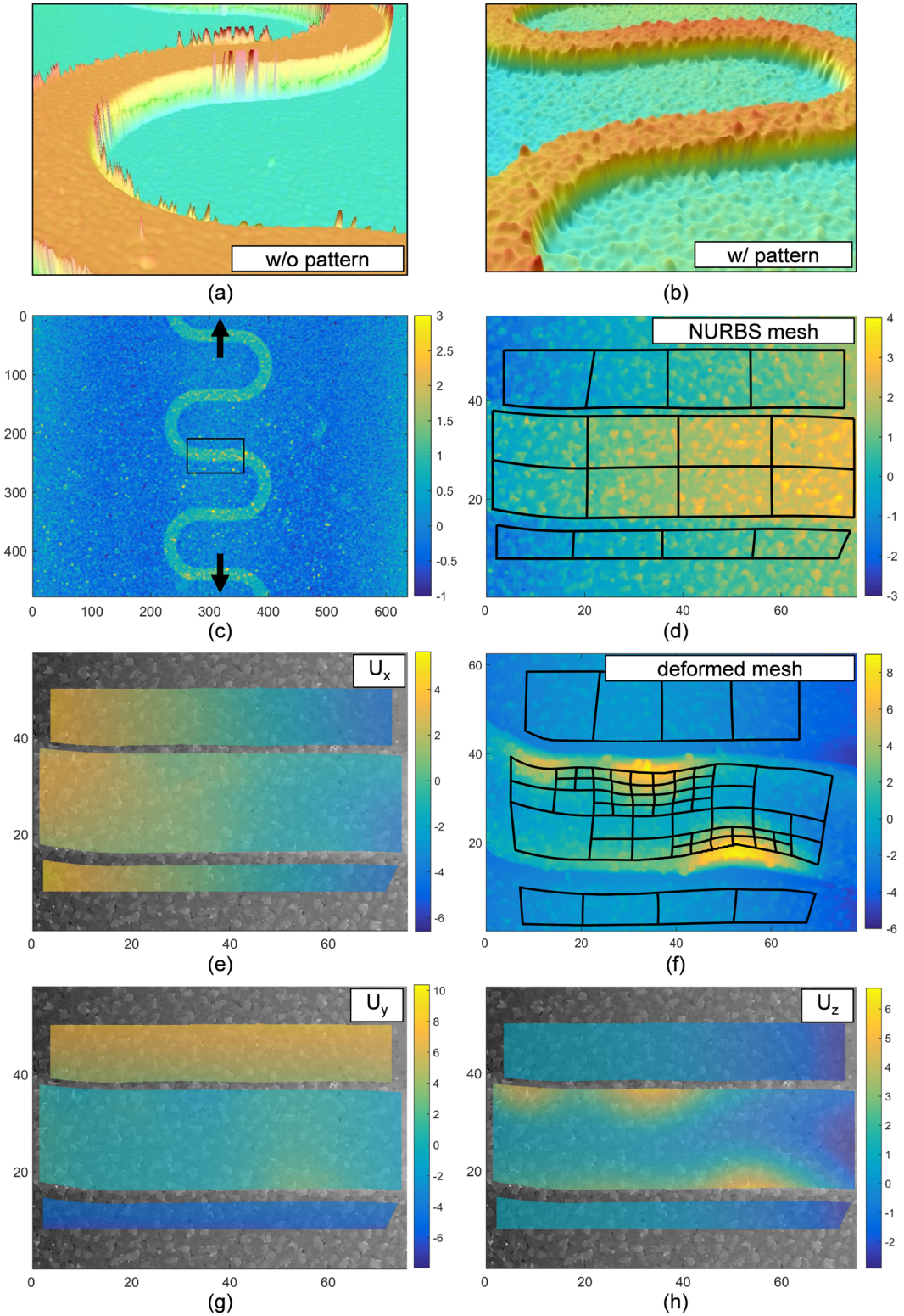

FIGURE 6 Characterisation of microscale deformation of stretchable electronics using self-adaptive isogeometric DHC of *in-situ* optical profilometry height data: 3D view of a topography of a meandering Al interconnect adhered to a PI foil substrate, (a) without and (b) with an applied InSn DIC pattern (Pattern **e** shown in Figure 3e). (c) Overview of the topography and testing condition (also showing the global tensile direction and the region of interest) of the interconnect. (d, f) Graphical representation of the NURBS mesh used for DHC, (d) the initial mesh drawn over the initial surface topography and (f) the self-refined mesh after convergence of the adaptive isogeometric DHC drawn in the deformed configuration over the final topography. (e, g, h) The successfully correlated 3D displacement fields, plotted in the reference configuration, consisting of the displacement field in (e) x, (g) y, and (h) z (out-of-plane) direction. All dimensions are in μm. DHC, digital height correlation; NURBS, non-uniform rational B-splines

edges of the deposited InSn islands and the Al interconnect structure are steep enough for a good DHC pattern but still smooth enough such that erroneous measurement points are prevented. An overview of the geometry of the Al interconnect on the PI substrate, the global tensile direction, and the considered region of interest is given in Figure 6c. Tensile experiments on the stretchable electronics samples were performed *in-situ*, using a Kammrath and Weiss microtensile stage under a Sensofar Plμ 2300 optical profilometre in confocal mode, with a 150× objective to obtain the highest possible magnification. The tensile test was conducted up to 40% applied global strain. For the stretchable interconnect structures, limited a priori knowledge regarding the 3D deformation of the samples upon stretching, especially the moment of buckling, was available. Therefore, "self-adaptive isogeometric DHC," as developed in Kleinendorst et al.,[49,50] is employed, that is, isogeometric shape functions are used for the representation of the 3D displacement fields (in a "global DIC" setting) in combination with a self-adaptive refinement procedure based on hierarchical refinement of the shape functions.* At the start of the deformation, a simple NURBS mesh is applied separately to the interconnect and the surrounding substrate on both sides, as shown in Figure 6d. During intermediate deformation steps (not shown here), the NURBS mesh is successfully refined in an automated fashion due to the localised behaviour, showing good convergence towards a low height residual (not shown). Figure 6f shows the final deformation step with a locally double-refined mesh drawn in the deformed configuration. The corresponding *x*-, *y*-, and *z*-displacement fields are given in Figure 6e,g,h, in the reference configuration, which shows an intricate buckling pattern. This 3D displacement field of the buckling pattern is quantitatively compared with multiscale Finite Element Method (FEM) simulations including cohesive zone interface elements to capture the delamination behaviour in Kleinendorst et al.[51] There it was found that this measured buckling pattern can be reproduced numerically by employing a higher fracture toughness in shear opening than in normal opening.

In Case Study II, we investigate the evolution of microplasticity and damage during deformation of a polycrystalline Fe foil, by performing an *in-situ* tensile test, using a Kammrath and Weiss microtensile stage, inside a Tescan Mira 3 SEM, employing in-beam SE imaging. The Fe foil was electro-polished in advance, to expose the microstructure. Subsequently, an InSn pattern was deposited on the surface, utilising the sputter deposition parameters according to Pattern **c** from Table 1. SEM scans of 3,096 × 3,096 pixels were taken before and during deformation (corresponding to a global strain of 1%, 2.5%, 3.5%, and 5%) over a 50 × 50-μm^2 FOV, resulting in a pixel size of ~16 nm. Figure 7a,b, respectively, shows the SEM images without deformation and at the last deformation step. We focus on one grain with a particular surface topology, which deforms the most during the experiment (as shown by the insets). In this grain, a high-quality DIC pattern is observed that nicely follows the locally steep surface topology. Importantly, the grain boundaries and triple junctions can still be seen through the pattern. This allows to easily find back the designated analysis region that was characterised before pattern application by, for example, electron backscatter diffraction (EBSD) (not performed here). Typically, during *in-situ* SEM testing, the contrast and brightness settings of the SE detector are adapted to counteract the reduction in contrast and brightness due to continuous electron beam-induced carbon deposition, also called carbon contamination. Here, however, the contrast and brightness settings are kept deliberately unchanged during the whole experiment to demonstrate the resilience of the DIC pattern against carbon contamination. For this case study including fracture, a "local," subset-based DIC analysis is the preferred choice, as material continuity is not assumed. A commercial DIC software package (VIC-2D from Correlated Solutions) was used to perform subset-based DIC on the SEM images, using a subset size and step size of, respectively, 21 and 1 pixel. Green–Lagrange strains are computed through nearest neighbour differentiation without filtering, essentially corresponding to a strain window of 1 data point. These settings correspond to a small "virtual strain gauge" (VSG) size of ~336 nm when using the formula of $L_{VSG} = (L_{window} - 1)L_{step} + L_{subset} = 21$ pixels proposed in Ref.[52] This results in the equivalent strain fields shown in Figure 7c,d,e,f. Localised deformation bands can be discerned with great detail, without any degradation of the pattern at 1% global strain. During further deformation, localisation continues, and the heterogeneity of the strain field increases significantly. Physical cracks appear in the foil; however, the correlation remains successful directly at the edges of the cracks, where strains of over 100% are measured. The occurrence of cracks has been confirmed by post-mortem SEM observation of the backside of the foil (not shown). The stability of the DIC pattern between fractured parts of the material can be of crucial importance when, for example, propagation of damage is studied, which is not trivial.[25] In the literature, a VSG size between 100 and 200 pixels (with an optimum at 141 pixels) is recommended

*In this procedure, non-uniform rational B-splines (NURBS), which can represent various geometrical shapes, are used for the shape functions and geometrical parametrization, offering high computational efficiency, accuracy, and robustness.[56] Upon localised deformation, the hierarchical refinement of the shape functions locally increases the number of degrees of freedom in an objective manner, by evaluation of the height residual obtained in the previous iteration.

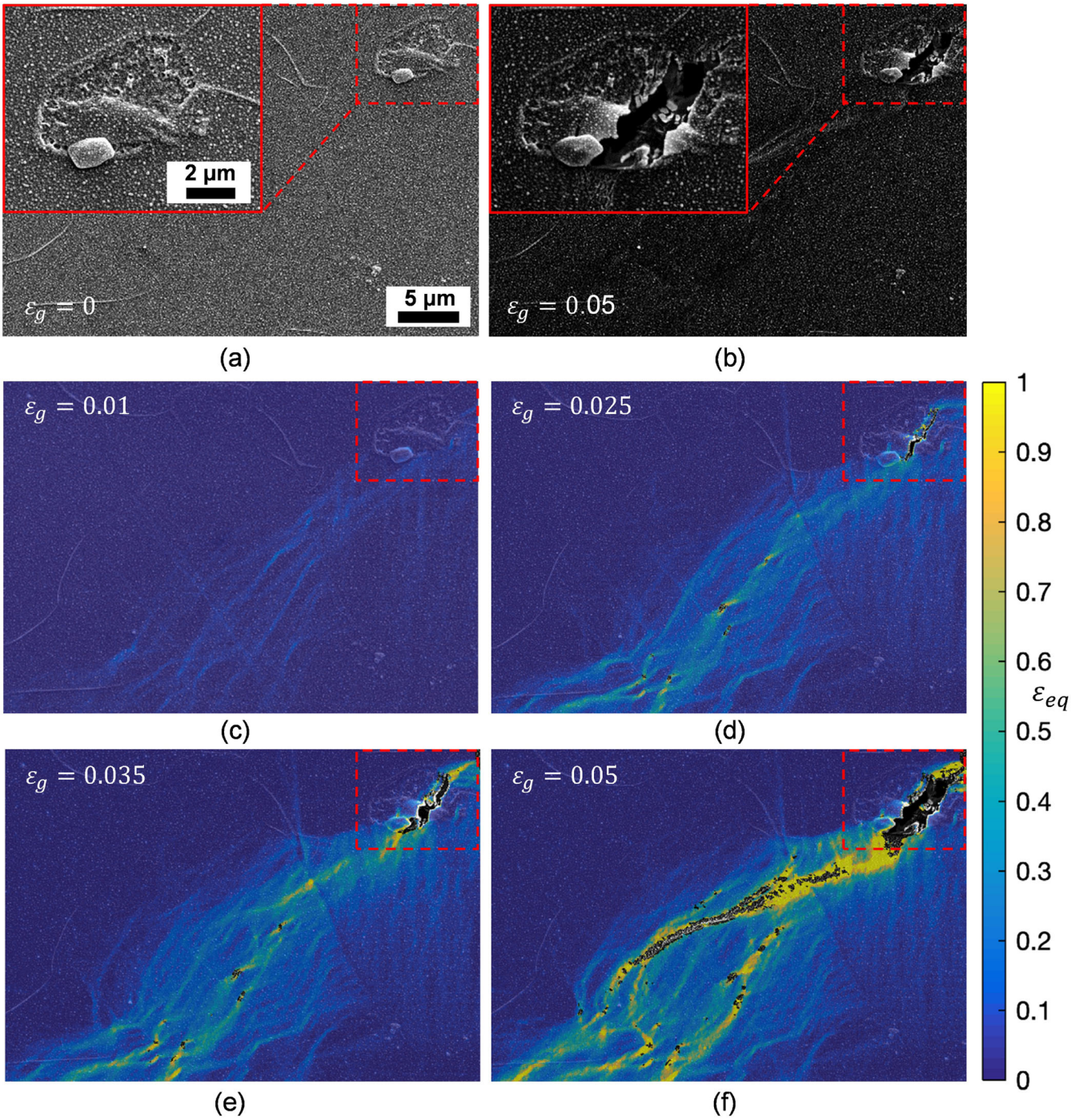

FIGURE 7 Overview of an *in-situ* SEM tensile test, processed by subset-based local DIC, on pure Fe, using in-beam SE scans. (a) Reference SEM scan at the start of the *in-situ* test, showing the InSn DIC pattern (created with the processing parameters of Pattern **c** from Table 1), directly deposited on the electro-polished surface of polycrystalline Fe, whereas the inset shows one particular grain. (b) The same area after uniaxial tension up to 5% global strain (with a large crack in the grain in the inset), subject to major loss of contrast due to contamination (contrast/brightness of the in-beam SE detector was not changed during the test). (c, d, e, f) The equivalent strain fields at, respectively, 1%, 2.5%, 3.5%, and 5% global strain, as computed by subset-based local DIC. DIC, digital image correlation; SE, secondary electron; SEM, scanning electron microscope

as a compromise between good image correlation stability for large VSG and good spatial resolution (with low underestimation of the maximum strain) for a small VSG.[53] With our pattern, however, high image correlation stability is achieved for a much smaller VSG (of 21 pixel). This provides the possibility to measure strains at a much higher spatial resolution in terms of pixels, whereas the images have been captured with a relatively small pixel size of ~16 nm (compared with most *in-situ* SEM testing publications).

4 | DISCUSSION: APPLICABILITY OF THE PATTERNING METHOD

For a DIC patterning technique, the suitability to various substrate materials is an important concern. In Table 1 and Figure 3, we show that Si and PI can be used, which proves that a conductive substrate material is not a requirement. Alternatively, Case Studies I and II demonstrate that Al and Fe are also suitable as a substrate. As with all forms of low-pressure deposition, the InSn adatoms will have a finite (i.e., nonzero) sticking probability on all surfaces; therefore, a pattern should form on all materials. The only real limitation is that the specimen does not damage or degrade in the environment of the sputter deposition process, that is, low pressure, electron charging, and mild ion bombartment, which limits the applicability to delicate and moisture-sensitive specimens such as biological samples and hydrogels. Moreover, it should be noted that the adatom surface diffusion length will not be equal for different materials; hence, the same deposition parameters cannot guarantee the exact same morphology and size of the InSn pattern for different substrate materials (even though Pattern **c** appears similar when deposited on Si and Fe). Therefore, for multimaterial samples, such as microelectronical components, it could potentially be more challenging to attain a highly homogeneous pattern, locally, over the different materials. Note that a continuous thin film of, for example, titanium[54] could be added underneath the InSn pattern to alleviate this concern, although care should be taken that such a continuous film can sustain the deformation of the underlying specimen inside localisation or damage zones.

We have not observed any direct effect of SEM imaging on the DIC pattern in terms of charging or local heating. For a continuous thin film, the electron beam energy may induce remodelling into separate islands to reduce the total energy of the system (similar to the concept of Au or Ag remodelling as discussed in Section 1); however, because the InSn is directly deposited in the low-energy configuration of separate islands, it is not surprising that this pattern is stable under electron beam imaging. Probably, however, the InSn pattern is not stable above its (low) melting temperature, thus restricting testing at higher temperature. There may be two options to circumvent this issue: (a) a nanometre thin layer of a material with higher melting temperature can be deposited on top of the InSn pattern, such that this thin film takes the shape of the underlying pattern and retains this during high temperature testing or (b) a sputtering material with a melting temperature above the testing temperature can be chosen, while assuring the island growth sputter deposition mode by performing the deposition at a temperature close to the melting temperature.

The InSn alloy shows great promise as room temperature sputtering material, yielding features from nanometre to micrometre size in a controllable manner. Nonetheless, there should be good alternatives for room temperature deposition and testing, for example, other low-melting temperature (solder) alloys such as 49Bi21In18Pb12Sn (melting temperature of 58°C). Finally, after the *in-situ* test has been finished, a detailed analysis of the substrate surface underneath the pattern is often of interest. To this end, a dedicated (electro-)chemical etching step for InSn, for example, the one suggested in Levy et al.,[55] may be employed to completely remove the pattern to enable, for example, post-mortem backscattered electron (BSE) and/or EBSD analysis.

5 | CONCLUSIONS

In this work, we demonstrate the feasibility of a relatively simple technique to obtain a controllable, high-quality DIC pattern for multi-microscopy testing, over a range of scales, on different substrates (Si, PI, Al, and Fe). Using a low-melting temperature (InSn) solder alloy, we provide the ability to create dense, high-quality DIC patterns over large areas with feature sizes ranging from ~10 nm to ~2 μm, without resorting to elevated substrate temperatures, challenging the most sophisticated patterning techniques available in the literature. The capability of controlling several properties of the pattern, such as feature size, size range, and shape, is achieved by changing two key sputter deposition parameters to fine tune the properties of the patterns. All DIC patterns considered here were imaged using scanning electron microscopy, showing good contrast in combination with a high, homogeneous feature density. Moreover, the finest pattern seems to have an optimal morphology for nanoscale DIC on AFM height profiles, whereas the patterns with larger features show good potential for multiscale DIC using a regular multiple-magnification optical microscope (or multiple optical cameras).

Finally, the robustness and applicability of the DIC patterns was tested on two challenging case studies. (a) A relatively new type of DIC method, that is, self-adaptive isogeometric DHC on optical surface height profiles, was investigated. For this method, which requires a very specific type of pattern (micrometre-sized speckles, good height contrast, and smooth slopes at the feature edges), it was demonstrated that a dedicated pattern could be deposited, yielding high-quality 3D surface deformation fields. (b) At the nanoscale, it can be challenging to elucidate complex microplasticity, damage, and fracture mechanisms during *in-situ* experiments, due to conflicting requirements of high spatial resolution of the

strain field and high robustness of the image correlation at high strain. It was demonstrated, for an *in-situ* SEM tensile test on a polycrystalline pure Fe foil, that the InSn DIC pattern with nanoscale features is ideal for sustaining and quantifying high local strains near fractured areas.

In summary, the high controllability and performance of DIC patterns created by PVD of a low-melting temperature solder alloy, which only requires a single deposition step with a conventional sputter deposition system, provide a promising step towards more routine *in-situ* DIC experiments that normally require highly optimised and complex patterning methods.

ACKNOWLEDGEMENTS

The authors greatly acknowledge Rob Fleerakkers, Chaowei Du, Sandra van de Looij-Kleinendorst, Uriel Hoeberichts, Jan Neggers, Philip Reu, Benoît Blaysat, Salman Shafqat, and Samaneh Isavand for their contributions and/or discussions. Part of this research was carried out under project number S17012b in the framework of the Partnership Program of the Materials Innovation Institute M2i (www.m2i.nl) and the Stichting voor de Technische Wetenschappen (www.stw.nl), which is part of the Netherlands Organisation for Scientific Research (www.nwo.nl).

ORCID

J.P.M. Hoefnagels https://orcid.org/0000-0001-8359-7575
T. Vermeij https://orcid.org/0000-0002-5434-6280

REFERENCES

[1] M. A., Sutton (**2008**). Digital image correlation for shape and deformation measurements. Springer handbook of experimental solid mechanics, 565–600

[2] B. Pan, K. Qian, H. Xie, A. Asundi, *Meas. Sci. Technol.* **2009**, *20*(6), 062001.

[3] J. Neggers, B. Blaysat, J. P. M. Hoefnagels, M. G. D. Geers, *Int. J. Numer. Methods Eng.* **2016**, *105*(4), 243.

[4] J. Littell, Large field digital image correlation used for full-scale aircraft crash testing: Methods and results, in *International Digital Imaging Correlation Society*, Springer, Cham **2017** 235.

[5] S. Yoneyama, H. Ueda, *Mater. Trans.* **2012**, *53*(2), 285.

[6] M. Bertin, C. Du, J. P. Hoefnagels, F. Hild, *Acta Mater.* **2016**, *116*, 321.

[7] D. Lunt, A. Orozco-Caballero, R. Thomas, P. Honniball, P. Frankel, M. Preuss, J. Q. da Fonseca, *Mater. Charact.* **2018**, *139*, 355.

[8] J. D. Carroll, W. Abuzaid, J. Lambros, H. Sehitoglu, *Int. J. Fatigue* **2013**, *57*, 140.

[9] A. P. Ruybalid, J. P. M. Hoefnagels, O. van der Sluis, M. P. F. H. L. van Maris, M. G. D. Geers, *Int. J. Solids Struct.* **2019**, *156*, 179.

[10] A. D. Kammers, S. Daly, *Exp. Mech.* **2013**, *53*(9), 1743.

[11] X. Wang, Z. Pan, F. Fan, J. Wang, Y. Liu, S. X. Mao, T. Zhu, S. Xia, *J. Appl. Mech.* **2015**, *82*(12), 121001.

[12] Y. Wang, P. Lava, S. Coppieters, P. V. Houtte, D. Debruyne, *Strain* **2013**, *49*(2), 190.

[13] L. I. J. C. Bergers, J. P. M. Hoefnagels, M. G. D. Geers, *J. Phys. D: Appl. Phys.* **2014**, *47*(35), 355306.

[14] X. Li, W. Xu, M. A. Sutton, M. Mello, *Mater. Sci. Technol.* **2006**, *22*(7), 835.

[15] Z. H. Xu, X. D. Li, M. A. Sutton, N. Li, *J. Strain Anal. Eng. Des.* **2008**, *43*(8), 729.

[16] B. K. Bay, T. S. Smith, D. P. Fyhrie, M. Saad, *Exp. Mech.* **1999**, *39*(3), 217.

[17] F. Hild, S. Roux, *Exp. Mech.* **2012**, *52*(9), 1503.

[18] M. Grédiac, F. Hild, *Full-field measurements and identification in solid mechanics*, Wiley-ISTE, London **2013**.

[19] J. Réthoré, *Int. J. Numer. Methods Eng.* **2010**, *84*(6), 631.

[20] A. P. Ruybalid, J. P. Hoefnagels, O. van der Sluis, M. G. Geers, *Int. J. Numer. Methods Eng.* **2016**, *106*(4), 298.

[21] F. Pierron, M. Grédiac, *The Virtual Fields Method: Extracting Constitutive Mechanical Parameters from Full-Field Deformation Measurements*, Springer Science & Business Media, Springer-Verlag New York **2012**.

[22] C. C. Tasan, J. P. Hoefnagels, M. Diehl, D. Yan, F. Roters, D. Raabe, *Int. J. Plast.* **2014**, *63*, 198.

[23] H. Ghadbeigi, C. Pinna, S. Celotto, J. R. Yates, *Mater. Sci. Eng., A* **2010**, *527*(18–19), 5026.

[24] J. Kang, Y. Ososkov, J. D. Embury, D. S. Wilkinson, *Scr. Mater.* **2007**, *56*(11), 999.

[25] C. C. Tasan, J. P. M. Hoefnagels, M. G. D. Geers, *Scr. Mater.* **2010**, *62*(11), 835.

[26] S. Bossuyt, Optimized patterns for digital image correlation, in *Imaging Methods for Novel Materials and Challenging Applications*, Vol. 3, Springer, New York, NY **2013** 239.

[27] B. Pan, Z. Lu, H. Xie, *Opt. Lasers Eng.* **2010**, *48*(4), 469.

[28] G. Crammond, S. W. Boyd, J. M. Dulieu-Barton, *Opt. Lasers Eng.* **2013**, *51*(12), 1368.

[29] W. A. Scrivens, Y. Luo, M. A. Sutton, S. A. Collette, M. L. Myrick, P. Miney, P. E. Colavita, A. P. Reynolds, X. Li, *Exp. Mech.* **2007**, *47*(1), 63.

[30] A. D. Kammers, S. Daly, *Meas. Sci. Technol.* **2011**, *22*(12), 125501.

[31] Y. L. Dong, B. Pan, *Exp. Mech.* **2017**, *57*(8), 1161.

[32] H. Hu, R. G. Larson, *Langmuir* **2005**, *21*(9), 3972.

[33] A. D. Kammers, S. Daly, *Exp. Mech.* **2013**, *53*(8), 1333.

[34] A. Githens, S. Daly, *Strain* **2017**, *53*(1), e12215.

[35] D. Yan, C. C. Tasan, D. Raabe, *Acta Mater.* **2015**, *96*, 399.

[36] F. Di Gioacchino, J. Q. Da Fonseca, *Exp. Mech.* **2013**, *53*(5), 743.

[37] S. H. Joo, J. K. Lee, J. M. Koo, S. Lee, D. W. Suh, H. S. Kim, *Scr. Mater.* **2013**, *68*(5), 245.

[38] A. Tatschl, O. Kolednik, *Mater. Sci. Eng., A* **2003**, *339*(1–2), 265.

[39] J. C. Stinville, M. P. Echlin, D. Texier, F. Bridier, P. Bocher, T. M. Pollock, *Exp. Mech.* **2016**, *56*(2), 197.

[40] C. B. Montgomery, B. Koohbor, N. R. Sottos, *Exp. Mech.* **2019**, *x*, 1. https://doi.org/10.1007/s11340-019-00487-2.

[41] J. W. Abraham, T. Strunskus, F. Faupel, M. Bonitz, *J. Appl. Phys.* **2016**, *119*(18), 185301.

[42] J.P.M., Hoefnagels, Chapter 9 "Temperature dependence study of the surface roughness evolution: surface diffusion processes during a-Si:H growth," PhD thesis "A novel diagnostic approach for studying silicon thin film growth," Eindhoven University of Technology, **2005**

[43] Y. S. Jung, D. W. Lee, D. Y. Jeon, *Appl. Surf. Sci.* **2004**, *221*(1–4), 136.

[44] J. C. Passieux, F. Bugarin, C. David, J. N. Périé, L. Robert, *Exp. Mech.* **2015**, *55*(1), 121.

[45] H. W. Schreier, D. Garcia, M. A. Sutton, *Exp. Mech.* **2004**, *44*(3), 278.

[46] J. Ning, S. Xu, Y. Wang, S. M. Lessner, M. A. Sutton, K. Anderson, J. E. Bischoff, *J. Biomech. Eng.* **2010**, *132*(12), 121010.

[47] J. Neggers, J. P. M. Hoefnagels, F. Hild, S. Roux, M. G. D. Geers, *Exp. Mech.* **2014**, *54*(5), 717.

[48] J. Van Beeck, J. Neggers, P. J. G. Schreurs, J. P. M. Hoefnagels, M. G. D. Geers, *Exp. Mech.* **2014**, *54*(4), 557.

[49] S. M. Kleinendorst, J. P. M. Hoefnagels, C. V. Verhoosel, A. P. Ruybalid, *Int. J. Numer. Methods Eng.* **2015**, *104*(10), 944.

[50] S. M. Kleinendorst, J. P. M. Hoefnagels, R. C. Fleerakkers, M. P. F. H. L. van Maris, E. Cattarinuzzi, C. V. Verhoosel, M. G. D. Geers, *Strain* **2016**, *52*(4), 336.

[51] S.M., Kleinendorst, R, Fleerakkers, E., Cattarinnuzzi, P., Vena, D., Gastaldi, M.P.F.H.L., van Maris, & J.P.M., Hoefnagels (**2019**). Experimental-numerical characterization of metal-polymer interface delamination in stretchable electronics interconnects. *Submitted for publication*.

[52] International Digital Image Correlation Society, E.M.C., Jones and M.A., Iadicol (Eds.) (**2018**). A good practices guide for digital image correlation. https://doi.org/10.32720/idics/gpg.ed1.

[53] P. Reu, *Exp. Tech.* **2015**, *39*(5), 1.

[54] S. M. Guo, M. A. Sutton, N. Li, X. D. Li, L. W. Wang, S. Rajan, *Exp. Mech.* **2017**, *57*(1), 41.

[55] S. A. Levy, Y. B. Kim, R. W. Kraft, *J. Appl. Phys.* **1966**, *37*(10), 3659.

[56] T. Elguedj, J. Réthoré, A. Buteri, *Comput. Methods Appl. Mech. Eng.* **2011**, *200*(1–4), 40.

How to cite this article: Hoefnagels JPM, van Maris MPFHL, Vermeij T. One-step deposition of nano-to-micron-scalable, high-quality digital image correlation patterns for high-strain *in-situ* multi-microscopy testing. *Strain*. 2019;e12330. https://doi.org/10.1111/str.12330